Application of atmospheric pressure plasma in environmental remediation and medicine

Kazunori Takashima, Hirofumi Kurita, Hachiro Yasuda and Akira Mizuno
Dept. of Environmental and Life Sciences
Toyohashi University of Technology
phone: (81) 532-44-6921
e-mail: takashima@ens.tut.ac.jp

***Abstract*— Discharge plasma technology is widely studied in various fields such as energy conversion, semiconductor devices, environmental protection, de-velopment of new materials, heat and light sources, surface finishing, biology, medicine and so on. We have studied the application of atmospheric pressure discharge plasma to environmental remediation, biology and medicine. In this paper, recent progress of our study on diesel exhaust cleaning, ammonia production, sterilization of bacteria, inactivation of viruses, medical care like cancer treatment will be introduced briefly.**

I. INTRODUCTION

Discharge plasma in gas phase produces energetic electrons, which can collide with neutral gas molecules to produce gas molecules in excited state, dissociated gas molecules, ions and electrons. These species can sometimes induce chemical reactions because they are reactive. Discharge plasma generated at atmospheric pressure using short pulse high voltage application or application of AC high voltage with dielectric barrier is non-thermal, in which most electric energy from the high voltage application is delivered to electrons. Therefore, temperatures of ions and neutrals are nearly the same as room temperature. The atmospheric pressure non-thermal plasma produced in this way is useful in many fields because of high energy efficiency, little heat damage to the object, simple structure and easy operation of plasma generator.

We have studied diesel exhaust cleaning, in which nitrogen oxides (NOx) and particulate matter (PM) should be removed. NOx was re-moved through selective catalytic reaction using ammonia (NH3-SCR)[1]. This process works well at high temperatures (normally 200-250 degree C) to reduce NOx into N2 and H2O but NOx removal efficiency is low at low temperatures[2] because of low catalytic activity at low temperatures. Therefore we employed non-thermal plasma in combination with NH3-SCR catalyst to enhance the reaction at low temperatures[3-7]. PM from diesel engine includes fine particles ranging from nano to micro meter in diameter[8-10]. A diesel particulate filter, which is

made of porous ceramics, is a de-facto standard for diesel PM removal but very high pressure drop cannot be avoided for the trapping of fine particles[11-12]. Regeneration of the filter, that is final treatment of PM deposited on a DPF through oxidation (com-bustion), is another problem to solve. Heat regeneration is normally used but it has a risk of thermal runaway because of the difficulty in precise temperature control. We investigated an elec-trostatic precipitator (ESP) to collect diesel PM, which has an advantage that fine par-ticles can be effectively collected without significant pressure drop. Simultaneous oxidation of the PM deposited on a collecting electrode in an ESP as well as the regeneration of a DPF with an assistance of discharge plasma was experimentally studied. Improvement of NH3 generation process is a subject to be studied for on-board NH3-SCR. NH3 is generated by spraying urea solution into exhaust gas in a commercial NH3-SCR system but it requires high temperature exhaust, which is not satisfied in some cases. We have studied NH3 genera-tion process at a moderate temperature using discharge plasma and a combination of discharge plasma and catalyst[13-17]. This method is interesting from a viewpoint of al-ternatives to Haber-Bosch process, which is a great breakthrough in the 20th century but it requires high temperatures and very high pressure.

Sterilization of bacteria or inactivation of viruses using non-thermal plasma is useful because they are room temperature processes and the heat damage to the object can be ignored. In addition, the process is simple and safe because of no usage of toxic chemicals and therefore no risk of its residue. Risk of emergence of drug-resistant strains should be neglected because bacteria are sterilized not by spe-cific interactions between the bacteria and some chemicals but possibly by non-specific oxidation due to reactive species (radi-cals) gener-ated by the plasma. We have studied the mechanisms of sterilization and inac-tivation experimentally[18-22]. Not only direct exposure to the plasma but also exposure to the water or the liquid medium preprocessed by discharge plasma was found to affect living cells. For example both the direct and indirect exposure to the plasma can induce cancer cell apoptosis suggesting that not only very short-life spe-cies directly generated by the plasma but also stable or meta-stable species generated through some chemical reactions in liquid phase are associated with the process. We have studied cellular responses to the water and cell culture medium that were prepared by exposing to atmospheric pressure plas-ma[23-25].

II. EXPERIMENTAL

A. Electrostatic charging and precipitation of diesel PM

Figure 1 shows a schematic diagram of the experimental setup for PM collection using an ESP and a DPF. The DPF was installed down-stream of the ESP. A diesel generator (SUBARU, SGD3000S-III) was used to generate PM. Exhaust gas flow rate was about 900L/min. Exhaust was sampled at downstream of the ESP-DPF combined reactor for PM number concentration measurement at a rate of 1L/min. The sampled exhaust was diluted with particle-free N_2 gas and then analyzed using an engine exhaust particle sizer (EESP; TST Ltd, 3090) to measure the number concentration of PM. Figure 2 shows a schematic illustration of the ESP combined with DPF used in this experiment. It consists of a 100mm-long and 36mm-diameter wire-cylinder type ESP and 128mm-long and 50mm-diameter DPF. Negative DC high voltage was applied to a discharge electrode made

of thin SUS wire (0.2mm in diameter) to generate corona discharge in the ESP.

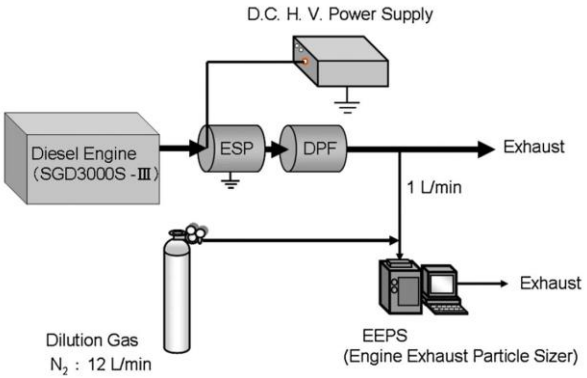

Fig. 1. Schematic diagram of an experimental setup.

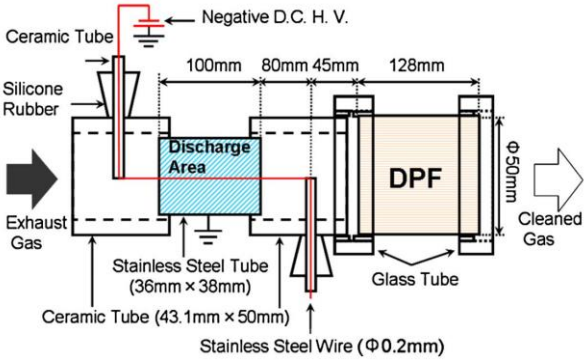

Fig. 2. Schematic illustration of an ESP combined with DPF.

B. Suppression of re-entrainment of collected PM

As was described above, ESP has some definite advantages over DPF. However, it has some problems as well. Re-entrainment of particles is one of the problems that arises especially for the application to diesel exhaust cleaning. When low-resistance particles such as diesel PM, which consists of carbon soot, are collected by an ESP, they lose the original charge and then they are charged oppositely on the collecting electrode. Once particles are oppositely charged they are detached from the collecting electrode and entrainment into gas stream due to electrostatic repulsive force. In this way, such particles are subjected to collection and entrainment repeatedly and finally emitted from an ESP. This is called "abnormal re-entrainment" and ESP sometimes cannot provide high performance for conductive particles due to this phenomenon.

We studied an effect of fine structure introduced on the surface of collecting electrode to cope with this problem. Collection electrode with fine structure can distort the electrostatic field near the surface probably affect the characteristics of particle re-entrainment. In ad-

dition, fine structure should work as a windbreak against gas stream just near the collecting electrode so that re-entrainment due to air flow should be suppressed.

Figure 3 shows a schematic illustration of an ESP used in this study. It has basically the same configuration as the one in the previous section but as a discharging electrode, a SUS rod equipped with some star-shaped electrodes were used in place of a SUS wire. In order to investigate the influence of the surface structure of the collecting electrode, a SUS mesh was installed on the colleting electrode to modify the surface roughness. Table 1 shows the properties of the mesh investigated in this study. A SUS plate having the same thickness as the stainless steel mesh was also examined to adjust the gap distance between the discharging electrode and the collecting electrode. In this experiment, only ESP was used.

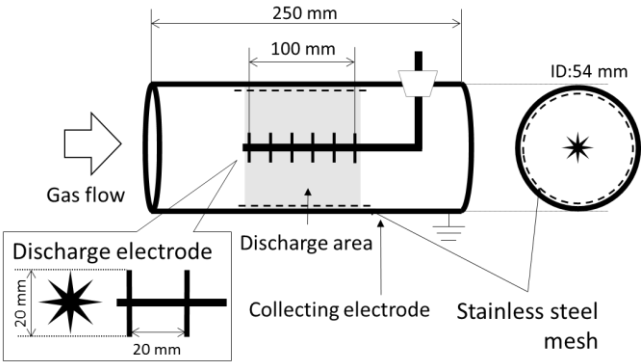

Fig. 3. Schematic illustration of an ESP having collecting electrode with fine structure..

TABLE 1: LIST OF SUS MESH FOR COLLECTING ELECTRODE SURFACE STRUCTURE MODIFICATION

Type (The number of holes par inch)	A [mm]	B [mm]	Open area [%]
16	0.29	1.30	66.9
18	0.34	1.07	57.6
30	0.25	0.60	49.8
40	0.18	0.46	51.7
120	0.08	0.13	38.3
SUS plate	--	--	0

C. Ammonia generation under moderate condition

Figure 4 shows a dielectric barrier discharge (DBD) reactor used for NH_3 generation. The reactor consists of a quartz glass tube, high voltage and grounded electrodes. Dielectric pellets were packed inside the glass tube. As a high voltage electrode, a stainless steel wire of 1.5mm in diameter was placed at the center of the tube. A stainless steel mesh was wrapped on the outer surface of the glass tube and grounded. DBD shown in figure 4(b) was generated by applying AC high voltage. Al_2O_3, TiO_2, $BaTiO_3$, CeO_2, Ru-Al_2O_3 were used as pellet packed in the reactor.

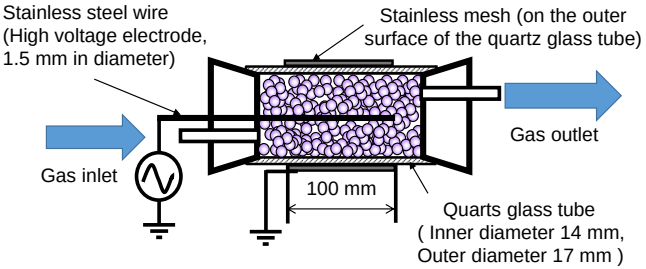

(a) DBD reactor

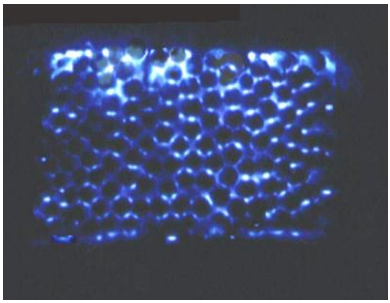

(b) DBD

Fig. 4. Schematic illustration of a DBD reactor.

Figure 5 shows a schematic diagram of an experimental setup. Starting gas was prepared by mixing N_2, NOx and CO and then H_2O content was adjusted by saturated water vapor. The gas was preheated before entering the DBD reactor, which was placed in a convection oven to control the temperature (120 degree C). Out gas was cooled to separate excess water content. Gas component was analyzed by FT-IR and liquid component was analyzed by ion chromatography. NH_3 concentration shown in this section is the sum of those detected in gas and liquid phases.

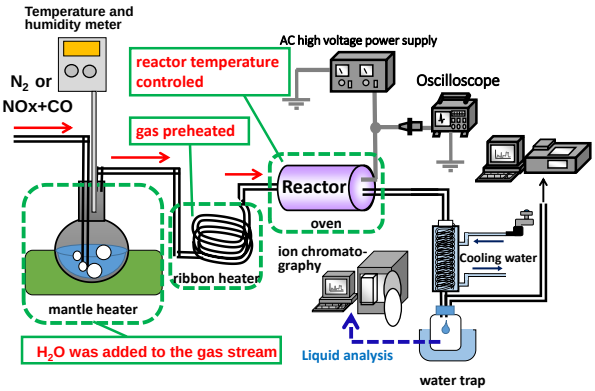

Fig. 5. Schematic illustration of an experimental setup for NH_3 generation using DBD.

D. Inactivation of viruses using DBD

There are many reports on bacteria and virus inactivation but its mechanism is not fully understood. We have developed a simple experimental system to investigate virus inactivation mechanism using discharge plasma. In this study, bacteriophage lambda (λ phage) shown in figure 6, which consists of double-stranded linear DNA and coat proteins and bacteriophage M13 (M13 phage) shown in figure 7, which consists of single-stranded circular DNA and coat proteins, were used as model virus having the simplest construction. The advantage of this experimental design is that both DNA and coat proteins of the plasma processed bacteriophage can be processed molecular biologically. Therefore, damages on DNA and coat proteins can be separately evaluated.

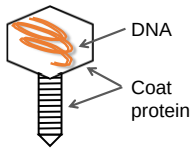

(a) Schematic illustration of λ phage

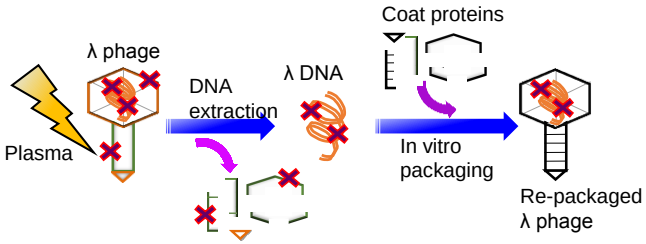

(b) Procedure of repackaging of λ phage

Fig. 6. Assay of λ phage using repackaging.

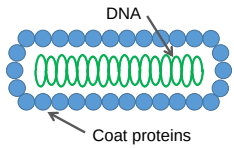

(a) Schematic illustration of M13 phage

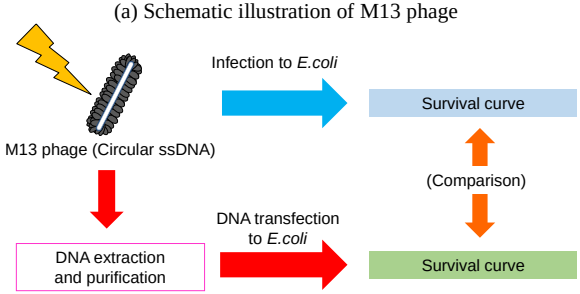

(b) Procedure of repackaging of M13 phage

Fig. 7. Assay of M13phage using repackaging.

Figure 8 shows a schematic illustration of DBD reactor used in this study. The peak-to-peak voltage and frequency of the AC high voltage and input power were 40kV$_{p\text{-}p}$, 2kHz and 8.7W, respectively. A 20μl aliquot of sample suspension was spotted and widely spread on a hydrophilically augmented PET film. Sample suspension was recovered from the PET film by adding 40μl of distilled water on the PET film after DBD application. The recovered λ phage was examined by infection to *E. coli* both as it was and after repackaging. Inactivation of M13 phage was analyzed by infection and transfection of extracted DNA to *E. coli*. Phage plaques of the infected *E. coli.* were counted after incubation at 40 degrees C for 24h.

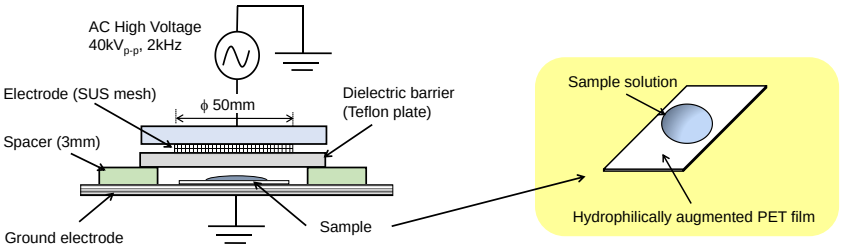

Fig. 8. DBD reactor for bacteriophage inactivation.

E. Cancer cell apoptosis induced by direct and indirect exposure to plasma jet

Atmospheric pressure plasma jet (APPJ) generates charged particles, reactive oxygen and nitrogen species, UV ray etc. APPJ is actively studied in the field of medical application with an interest of interaction between cells and APPJ or water and medium that are irradiated by APPJ. We have investigated chemical species generated in the plasma-treated cell culture medium and cancer cell response when it was exposed to the plasma-treated medium. Figure 9 shows APPJ generator. It consisted of a quartz glass tube as a dielectric barrier, a thin SUS wire as a high voltage electrode and a SUS mesh as a grounded electrode. By applying pulsed high voltage in the presence of Ar gas flow, DBD was generated and luminous APPJ was generated from the end of the glass tube. Amplitude, pulse width and repetitive frequency of the applied voltage were 12kV$_{0\text{-}p}$, 2.8μsec, 2.5kHz, respectively. Ar gas flow rate was 2L/min. H_2O_2 concentration in plasma treated medium was measured using *Amplex Red* reagent and nitrate and nitrite ions were measured by 2 3-diaminonaphthalene assay. Two human lung cancer cell lines, A549 and NCI-H460 were used to investigate the response of cancer cell plasma-exposed cell culture medium. Viability and cytotoxicity were simultaneously measured by two protease activities associated with viability and cytotoxicity, respectively. Cell apoptosis were measured by caspase 3/7 acitivities.

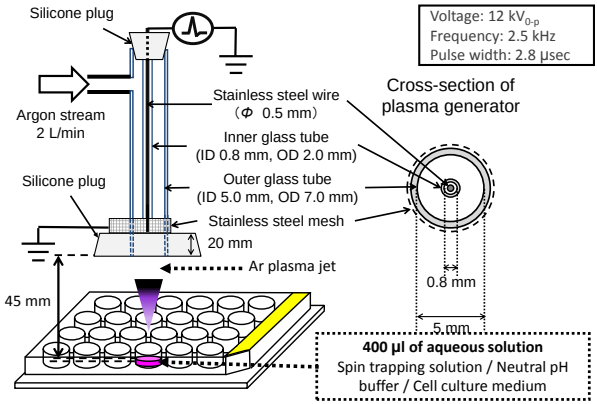

Fig. 9. Schematic illustration of APPJ generator.

III. RESULTS AND DISCUSSION

A. Electrostatic charging and precipitation of diesel PM[26-27]

Figure 10 shows a number concentration and its size distribution of PM in raw diesel exhaust used in this study. A diesel generator was operated at nearly full load (2.6kW load against 3.0kW capacity) to obtain dry PM with little soluble organic fraction (SOF). The figure shows a peak at about 70nm in diameter and most PM was smaller than 200nm.

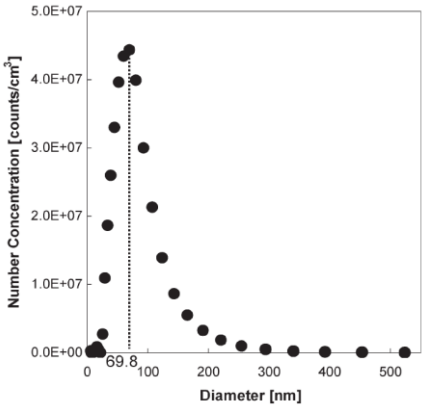

Fig. 10. Number concentration and size distribution of PM in raw diesel exhaust.

Figure 11 shows time change of PM removal ratio when only ESP was operated (DPF was not installed). The applied voltage to the ESP was -12.5kV and the resulting current ranged from -0.45mA to -1.25mA. Removal ratio was calculated from the data when ESP was on and off. The number concentrations at 69.8nm of diameter, where the size distribution has a peak, was used for calculating PM removal ratio unless otherwise noted in this

section. Approximately 95% of the PM was removed when the ESP was on.

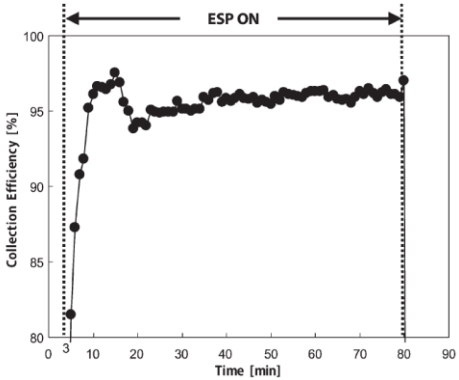

Fig. 11. Time change in PM concentration (at 69.8nm in diameter) when ESP was on.

Figure 12(a) shows PM removal ratio using ESP-DPF combined system when ESP was on and off. The ESP was operated under the same condition as figure 11. Around 98% of the removal rate was obtained when ESP was off, meaning the removal rate of DPF alone. When ESP was on, removal ratio nearly 100% was obtained suggesting that fine PM was completely removed by the combination of ESP and DPF. Assuming that ESP and DPF work independently, PM penetration ratio when both ESP and DPF is used can be estimated from the removal ratios of ESP and DPF as follows:

$$X_{E+D} = X_E \times X_D = 0.05 \times 0.02\ [-] = 0.1[\%]$$

where X_E and X_D are the penetration ratios of a single use of ESP and DPF respectively. Figure 12(b) shows averaged penetration ratio during the simultaneous operation of ESP and DPF was about 0.024%, which is significantly smaller than the above estimated value, suggesting a certain synergetic effect of simultaneous operation of ESP and DPF.

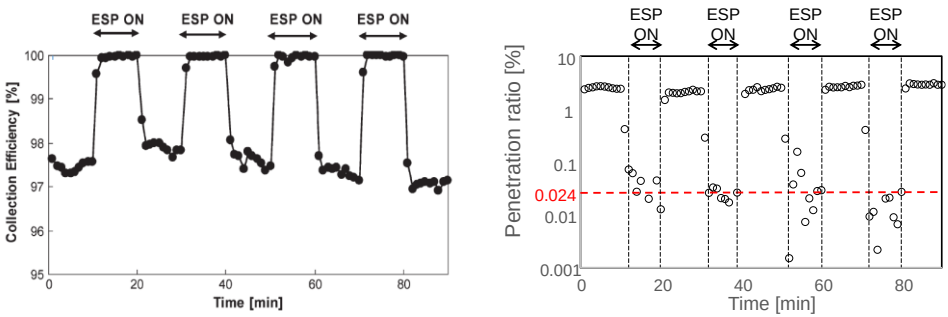

(a) removal ratio (b) penetration ratio

Fig. 12. Removal and penetration ratios of diesel PM using ESP-DPF combined system when ESP was on and off.

In order to investigate the agglomeration of diesel PM during passing through the ESP, exhaust was filtered by a quartz fiber filter at downstream of the ESP and observed with SEM. Figure 13 shows SEM images of a quartz fiber filter. No particle was observed on a new filter (a). Small particles were observed on a filter that through which diesel exhaust was filtered without operating the ESP (b). When ESP was on, a number of particles were collected on a filter (c). It is also found that particles formed secondary structure like a tree and that particles as large as a few micron were observed (d). These results suggest that primary particles can agglomerate in ESP probably because particles are subjected to the process of collection and re-entrainment repeatedly. Therefore, ESP can be said to work not only as a collecting device but also an agglomerating device.

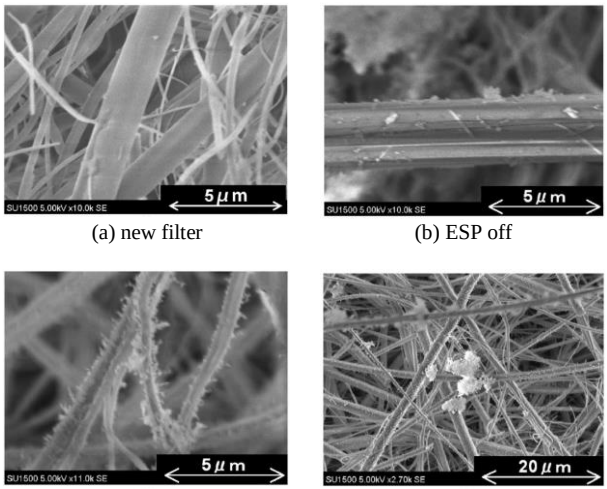

(a) new filter (b) ESP off

(c) ESP on (d) ESP on

Fig. 13. SEM images of the PM collected on a quartz fiber filter.

Figure 14 shows a time-lapse change of the pressure drop of the ESP-DPF combined system. Pressure drop across the DPF rapidly (4.7kPa /min) increased with time in an exponential manner when ESP was not operated. On the other hand, pressure drop increased very gradually (0.08kPa/min) when ESP was on. Increase in the pressure drop means the blocking of DPF because the pressure drop arises only in the DPF in this case. Therefore, simultaneous operation of the ESP at upstream the DPF significantly reduced blocking of the DPF. The significant difference in filter blocking speed by a factor of approximately 50 should be resulted from the difference in particle agglomeration. As was mentioned above, the number fine particles reduced and small number of large particles were found at downstream of ESP when ESP was on. Such large particles should be collected just on the DPF surface less closely so that blocking of the small pore of the DPF should be suppressed. On the other hand, a number of fine particles can penetrate deeply inside the pore so that the pore is packed with fine particles densely, resulting in significant and rapid increase in pressure drop.

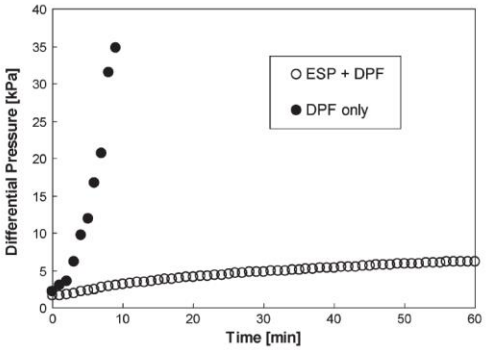

Fig. 14. Time-lapse change in pressure drop across DEP with and without simultaneous operation of ESP.

B. Suppression of re-entrainment of collected PM[28-29]

ESP was operated with negative high voltage of -10kV. Diesel generator was operated at middle load (1.8kW load against 3.0kW capacity) and the exhaust temperature was adjusted to 60°C by forced air cooling. Figure 15 shows photos of the SUS mesh placed on the collecting electrode. PM deposition significantly varied with the type of mesh. Generally, PM deposited on coarse meshes has highly branched structure like a tree but PM deposited on fine meshes has even and flat structure.

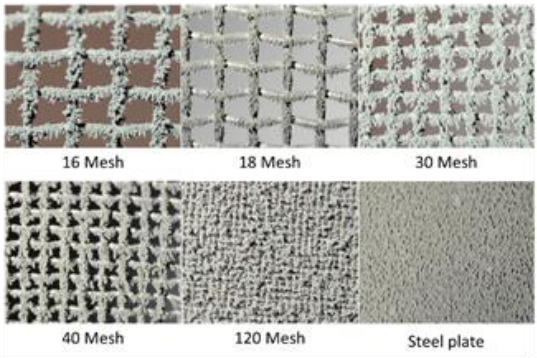

Fig. 15. Photographs of SUS mesh and SUS plate installed on the collecting electrode of ESP.

Figure 16 shows PM removal efficiency of each mesh 10 minutes after the starting the experiment. In any cases using collecting electrode having rough surface showed higher PM removal rate compared with that of normal ESP. The 18 mesh showed the highest removal efficiency of 91.6%. But unexpectedly, particle deposition on the 18 mesh was least significant. From these result we can assume that the particles were collected in the narrow space between the mesh and the collecting electrode in this case in the following way: Particles are collected on a mesh element and the coagulated particles entered the space between the mesh and the collection plate, where abnormal re-entrainment into the gas stream is unlikely to occur. Ionic wind going toward the collecting electrode might helped falling down of the coagulated particles into the narrow space. In addition, collection effi-

ciency was significantly affected by types of mesh suggesting that roughness of the collecting electrode affect the "PM intake" phenomenon. Further investigation should be carried out to analyze the correlation of the surface roughness of the collecting plate and the collection efficiency so that we can elucidate the mechanism.

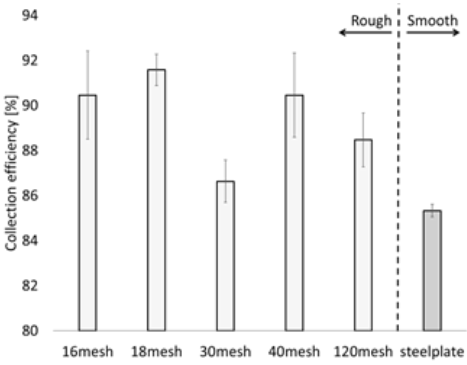

Fig. 16. Comparison of PM removal efficiency among various meshes.

C. Ammonia generation under moderate condition[13-14]

Figure 17 shows NH_3 and NOx concentration generated by using DBD reactor packed with various catalyst. When Ru supported on Al_2O_3 was used as catalyst and the starting gas contained CO, but NH_3 was generated but significant NH_3 generation was not observed in other experimental condition. No NH_3 was generated without DBD plasma suggesting that NH_3 was generated through plasma catalytic reaction in which CO plays an important role. Figure 18 shows correlation between NH_3 concentration and water content when Ru-Al_2O_3 was used in the presence of 1000ppm CO. The highest NH_3 concentration was observed when water content was 1.2%. NH_3 generation was low when water content was low probably because of too little hydrogen atoms and NH_3 generation was low when water content was high probably because of much oxygen atoms. CO could have worked as a scavenger of oxygen atoms by reacting with oxygen atom to form CO_2.

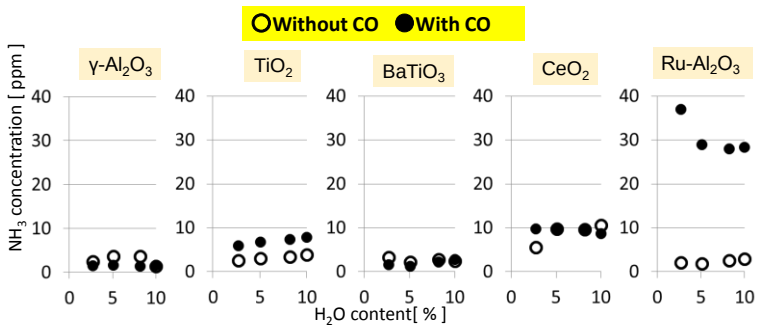

Fig. 17. Concentration of NH_3 generated by DBD and various catalyst pellets with and without CO (1000ppm).

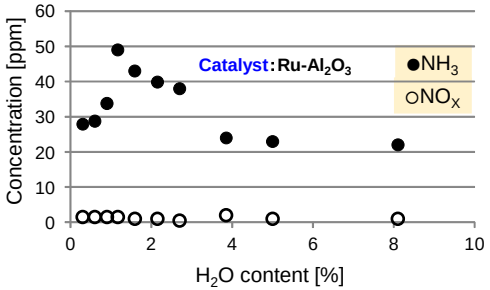

Fig. 18. NH_3 and NOx concentration vs water content when Ru-Al_2O_3 catalyst was used with CO (1000ppm) addition.

From the experiment on NH_3 generation from H_2 and N_2 or NOx, we found that NOx to NH_3 conversion is significantly higher than N_2 to NH_3 conversion. We examined NH_3 generation in N_2-NOx-CO-H_2O system. The same experimental setup as above was used but NO and NO_2 was supplemented to the starting gas. Various catalyst was examined and Pt-Rh supported on Al_2O_3 had the highest catalytic activity (data not shown here). Figure 19 shows NH_3 and NOx concentration in out gas when NO was supplemented to starting gas. When CO concentration was decreased from 1000ppm and NO concentration was increased from 0ppm at the same time, NH_3 concentration in the out gas increased with NO concentration and reach a highest value of 192ppm at CO and NO concentrations of 800ppm and 400ppm respectively. Further increase in CO concentration and further decrease in NO concentration resulted in decrease in NH_3 generation. NOx concentration was nearly 0ppm when CO concentration was more than 800ppm and NO concentration was less than 400ppm, where NH_3 generation was highest. These result suggest that NH_3 was generated from NO more effectively compared with N_2 and NOx generation was negligible when sufficient amount of CO was present.

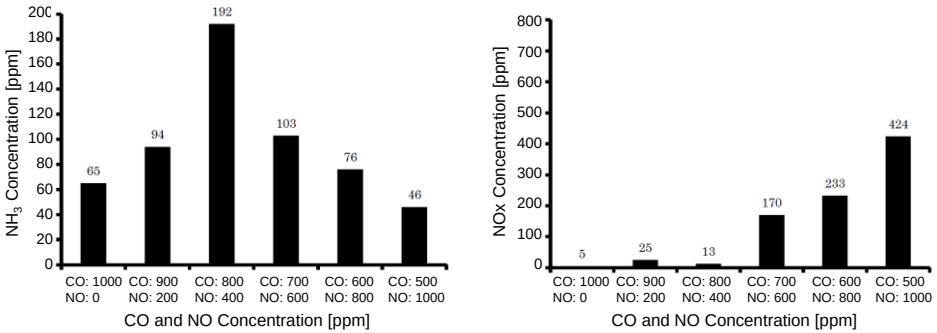

(a) NH_3 concentration (b) NOx concentration

Fig. 19. NH_3 and NOx concentration for various CO/NO ratio.

Figure 20 shows NH_3 and NOx concentration in out gas when NO_2 was added to starting gas. NH_3 generation showed similar dependency on CO/NO_2 ratio as CO/NO dependency but NH_3 generation dropped very sharply to 0ppm when NO_2 concentration exceeded

400ppm. Similarly, NOx generation increased more significantly with increasing NO_2 concentration compared with the case of NO addition. These results suggest that NO_2 is more reactive than N_2 to generate NH_3 but more oxidative, which can inhibit NH_3 generation in the presence of excessive amount of NO_2.

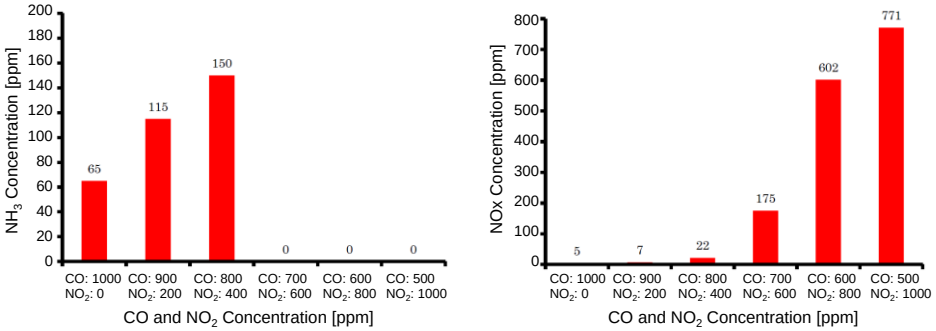

(a) NH_3 concentration (b) NOx concentration

Fig. 20. NH_3 and NOx concentration for various CO/NO_2 ratio.

D. Inactivation of viruses using DBD[18, 21]

Figure 21 shows inactivation characteristics of the λ phage. Infectivity of the plasma processed λ phage decreased rapidly with plasma exposure time and inactivated by a factor of 10^{-6} after 20sec. Damage associated with this inactivation should exist in DNA or coat proteins or both of them. On the other hand, repackaged λ phage, of which coat proteins were renewed after plasma exposure and therefore the phage has no damage on coat proteins, showed significantly gradual inactivation characteristics. Only 1 order of magnitude of inactivation was observed for the repackaged λ phage. This significant difference should be resulted from the difference in damage on coat proteins suggesting that plasma inactivation of λ phage is mostly attributed to damage on coat proteins.

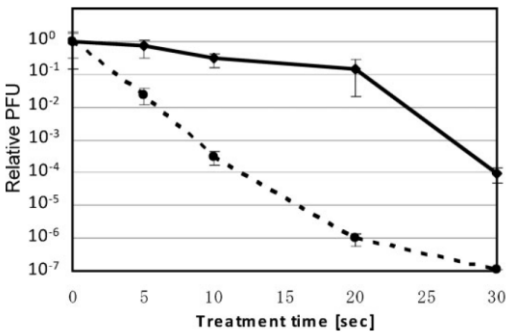

Fig. 21. Infectivity of λ phages subjected to the atmospheric pressure DBD.

Figure 22 shows electrophoretic analysis of coat protein and DNA of the plasma exposed λ phage. From figure 22(a), coat protein has no significant decrease in amount until

20sec of plasma exposure, which significantly inactivated λ phage. However the major band in figure 22(a) gradually shifted to upper side with the exposure time. These result suggest that exposure to the plasma caused some chemical modification to the coat proteins. From figure 22(b), DNA was not seriously damaged until 20sec of plasma exposure similar to the coat protein. This result agrees well with the result of infectivity of the repackaged λ phage. Judging from these results, plasma inactivation of λ phage is probably induced by chemical modification of the coat proteins.

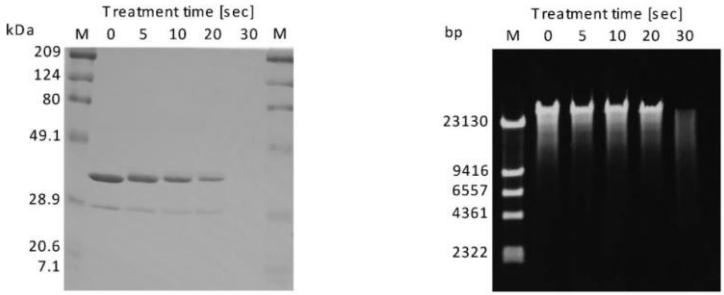

(a) Coat proteins (b) DNA

Fig. 22. Electrophoretic analysis of coat protein and DNA of the plasma exposed λ phage.

Figure 23 shows inactivation characteristics of the M13 phage. Unlike λ phage, both infection of plasma exposed M13 phage and transfection of the DNA extracted from the plasma processed M13 phage showed similar curves. The inactivation of transfected DNA was resulted from the only damage on DNA itself while inactivation of M13 phage were induced by damages on both DNA and coat proteins. Therefore, little difference between them suggests that with regards to the plasma inactivation of M13 phage, damage on the coat protein is comparable or negligible compared with damage on DNA. Opposite to λ phage, DNA damage played a significant role in inactivating M13 phage probably because single-stranded DNA of M13 phage is very fragile and it is damaged easily and significantly.

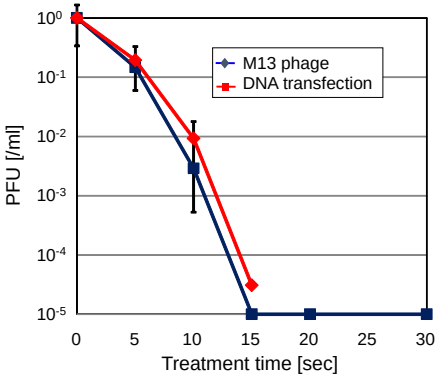

Fig. 23. Infectivity of M13 phages subjected to the atmospheric pressure DBD.

E. Cancer cell apoptosis induced by direct and indirect exposure to plasma jet[30]

Figure 24 shows H_2O_2, NO^-, NO_2^- concentrations in the cell culture medium exposed to APPJ for 10min. Gap between APPJ generator and the medium was 45mm and the applied voltage was $12kV_{0\text{-}p}$. From these results carried out using serially diluted plasma exposed medium, concentrations of H_2O_2, NO^-, NO_2^- in undiluted medium were estimated at 0.3mM, 0.3mM and 0.03mM, respectively. From a viewpoint of quantity, H_2O_2 and NO^- are the major species produced in plasma-exposed medium.

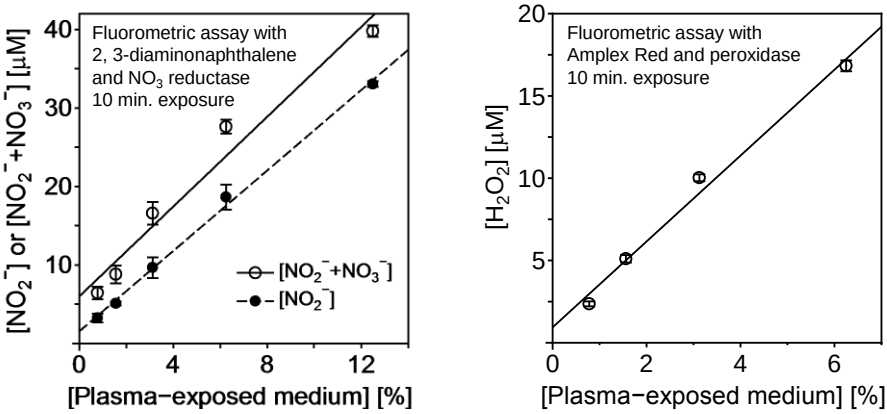

(a) NO^- and NO_2^- concentration (b) H_2O_2 concentration

Fig. 24. H_2O_2, NO^-, NO_2^- concentrations in the cell culture medium exposed to APPJ.

Then we investigated cellular responses to the plasma-exposed medium. Figure 25 shows cellular responses of two different human lung cancer cell lines (A549 and NCI-H460) after 8-hour culture in the various concentrations of plasma-exposed medium (solid line). Dotted line shows the cellular response when they were cultured in medium supplemented with H_2O_2, which was not exposed to APPJ. Cell viability relative to that of untreated cell (UTC) was plotted on the left vertical axis. Indexes of apoptosis and cytotoxicity relative to UTC were plotted on the right vertical axis. A549 and NCI-H460 showed qualitatively similar but quantitatively different response to the concentrations of plasma-exposed medium and H_2O_2. The first and the second horizontal axes are calibrated to each other. Viability reduced with increase in concentrations of plasma-exposed medium and H_2O_2. Apoptosis and cytotoxicity seems to have a threshold for the concentrations of plasma-exposed medium and H_2O_2. Figure 26 shows cell responses (viability, apoptosis and cytotoxicity indexes) of human lung cancer cell lines A549 and NCI-H460 after 16-hour culture. These results shows similar tendency as figure 26. It is interesting to point out that all the cellular responses (viability, apoptosis and cytotoxicity) investigated in this study can be accounted for by H_2O_2 concentration in the medium not depending on how the medium was prepared. It was strongly suggested that effect of plasma-exposed medium on these cancer cell lines is mainly ascribable to H_2O_2.

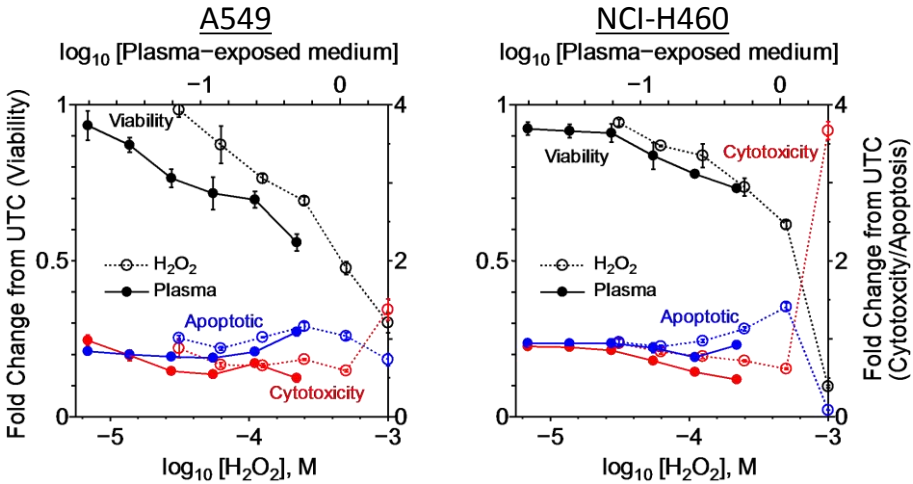

(a) A549 (b) NCI-H460

Fig. 25. Cellular responses of human lung cancer cell lines after 8 hours.

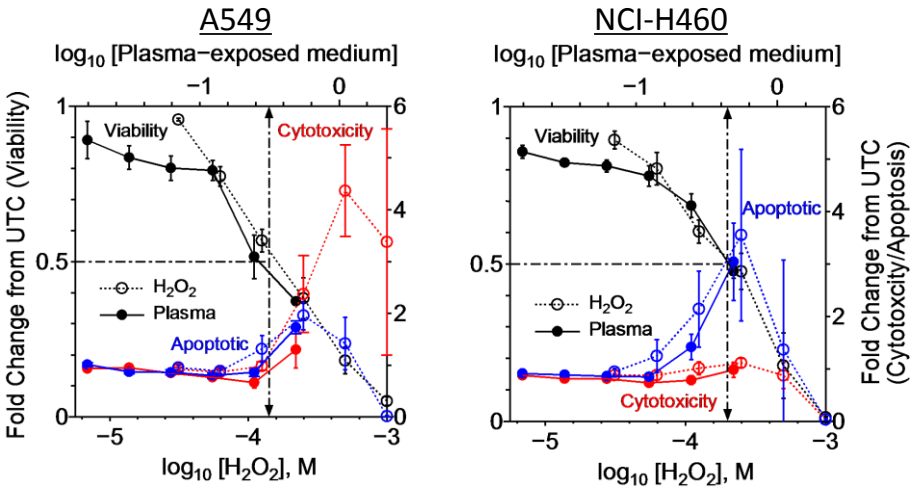

(a) A549 (b) NCI-H460

Fig. 26. Cellular responses of human lung cancer cell lines after 16 hours.

IV. Conclusion

Combination of electrostatic precipitator (ESP) and diesel particulate filter (DPF) were found effective for diesel PM collection because it significantly reduced pressure drop increase associated with blocking of DPF probably because of coagulation of PM due to abnormal re-entrainment in ESP. Fine structure introduced by a SUS mesh placed on the surface of collection electrode of ESP enhanced PM removal ratio possibly because of PM transfer into the narrow space between SUS mesh and collecting electrode. Plasma catalytic NH_3 generation from N_2 and H_2O was significantly enhanced by adding NO and CO suggesting that NO reacts with H_2O effectively in the presence of CO. Plasma inactivation of λ and M13phages were induced by fatal damage of coat proteins and DNA, respectively depending on the difference in nature of double-stranded and single-stranded DNA. Cellular responses in both A549 and NCI-H460 human lung cancer cell lines showed that the plasma-exposed medium and the H_2O_2 treatment gave similar reduction in viability and induction of apoptosis. Thus, H_2O_2 should be the major cause of these cellular responses.

References

[1] T. Johnson, "Diesel Emission Control in Review", SAE Technical paper, 2001-01-0184 (2001).
[2] M. Okubo et al., "Air and water pollution control technologies using atmospheric pressure low-temperature plasma hybrid process", J. Plasma Fusion Res., Vol.189, pp.152-157 (2013).
[3] K. Takashima et al., "Honeycomb Discharge Generated with a Single High Voltage Power Supply for Activating Catalyst", International Journal of Plasma Environmental Science and Technology, Vol.7, pp.142-147 (2013).
[4] J. Jolibois et al., "NOx Removal Using a Non-thermal Surface Plasma Discharge Powered by a Modulated Voltage", International Journal of Plasma Environmental Science and Technology, Vol.6, pp.74-80 (2012).
[5] S. Sato et al., "The study of NOx reduction using plasma-assisted SCR system for a heavy duty diesel engine", SAE Technical Paper, 2011-01-0310 (2011).
[6] S. Sato et al., "NOx Removal of Simulated Diesel Exhaust with Honeycomb Discharge", International Journal of Plasma Environmental Science and Technology, Vol.4, pp.18-23 (2010).
[7] S. Sato et al., "Honeycomb discharge for diesel exhaust cleaning", Journal of Electrostatics, Vol.67, pp.77-83 (2009).
[8] D.B. Kittelson, "Engines and nanoparticles: A review", J. Aerosol Sci., Vol.29, pp.575-588 (1998).
[9] H. Burtscher, "Physical characterization of particulate emissions from diesel engines: A review", J. Aerosol Sci., Vol.36, pp.896-932 (2005).
[10] M.M. Maricq, "Chemical characterization of particulate emissions from diesel engines: A review", J. Aerosol Sci., Vol.38, pp.1079-1118 (2007).
[11] J. Adler, "Ceramic diesel particulate filters", Intl. J. Appl. Ceramic Technology, Vol.2, pp.429-439 (2005).
[12] M. Okubo et al., "Low-temperature soot incineration of diesel particulate filter using remote nonthermal plasma induced by a pulsed barrier discharge", IEEE Trans. on Industry Appl., Vol.40, pp.1504-1512 (2004).
[13] T. Shimoda et al. "Ammonia Production Using Packed Bed Electric Discharge and Catalyst", presented at the ISPlasma2015 / IC-PLANTS2015, Nagoya, Japan, March 26-31, 2015, A4-P-18. (2015).
[14] K. Yamasaki et al., "Ammonia generation using electric discharge plasma generated in steam", International Journal of Plasma Environmental Science and Technology, vol.8, pp.113-116 (2014)
[15] G. Prieto et al., "Dielectric barrier discharge for ammonia production", Plasma Chemistry and Plasma Processing, Vol.33, pp.337-353 (2013).
[16] Y. Iitsuka et al., "Ammonia production from solid urea using non-thermal plasma", IEEE Transactions on Industry Applications, Vol.48, pp.872-877 (2012).
[17] S. Mededovic Thagard et al., "Analysis of the By-Products in the Ammonia Production From Urea by Dielectric Barrier Discharge", IEEE Transactions on Plasma Science, Vol.37, pp.444-448 (2009).

[18] Y. Tanaka et al., "Analysis of the inactivation mechanism of bacteriophage φX174 by atmospheric pressure discharge plasma", IEEE Transactions on Industry Applications, Vol.50, pp.1397-1401 (2014).
[19] T. Nakajima et al., "The Relation of E. coli Growth Phase and Low-Temperature He Plasma Jet Exposure", International Journal of Plasma Environmental Science and Technology, Vol.6, pp.189-193 (2012).
[20] T. Nakajima et al., "Generation of Bactericidal Factors in the Liquid Phase and Approach to New Gene Transfer Technology by Low Temperature Plasma Jet Treatment", International Journal of Plasma Environmental Science and Technology, Vol.5, pp.42-49 (2011).
[21] H. Yasuda et al., "Biological evaluation of DNA damage in bacteriophages inactivated by atmospheric pressure cold plasma", Plasma Processes and Polymers, Vol. 7, pp.301–308 (2010).
[22] H. Yasuda et al., "States of Biological Components in Bacteria and Bacteriophages during Inactivation by Atmospheric Dielectric Barrier Discharges", Plasma Processes and Polymers, Vol.5, pp.615-621 (2008).
[23] H. Kurita et al., "Use of molecular beacons for the rapid analysis of DNA damage induced by exposure to an atmospheric pressure plasma jet", Applied Physics Letters, Vol.107, 263702 (5 pp.) (2015).
[24] H. Kurita et al., "Radical reaction in aqueous media injected by atmospheric pressure plasma jet and protective effect of antioxidant reagents evaluated by single-molecule DNA measurement", Japanese Journal of Applied Physics, Vol.53, 05FR01A (4 pp.) (2014).
[25] K. Sano et al., "Evaluation of reactive oxygen species in non-thermal plasma-treated water", International Journal of Plasma Environmental Science and Technology, Vol.8, pp.149-153 (2014).
[26] H. Hayashi et al., "Collection of Diesel Exhaust Particles using Electrostatic Charging prior to DPF and Regeneration of DPF using Sliding Discharge", International Journal of Plasma Environmental Science and Technology, Vol.6, pp.160-165 (2012).
[27] H. Hayashi et al., "Electrostatic Charging and Precipitation of Diesel Soot", IEEE Transactions on Industry Applications, Vol.47, pp.331-335 (2011).
[28] M. Takasaki et al. "Electrostatic precipitation of diesel PM at reduced gas temperature", IEEE Transactions on Industry Applications, submitted.
[29] M. Takasaki et al. "Improvement of Collection Efficiency for Diesel Particulate Matter Installed with Ceramic Foam on a Collection Plate of an Electrostatic Precipitator", presented at the ISPlasma2015 / IC-PLANTS2015, Nagoya, Japan, March 26-31, 2015, A4-P-11. (2015).
[30] H. Kurita et al. "ROS detection and cellular responses induced by atmospheric pressure plasma exposure", presented at the ISPlasma2015 / IC-PLANTS2015, Nagoya, Japan, March 26-31, 2015, D4-O-06. (2015).